Mapping the human footprint from satellite measurements in Japan

著者	Yang Fan, Matsushita Bunkei, Yang Wei, Fukushima Takehiko
journal or publication title	ISPRS journal of photogrammetry and remote sensing
volume	88
page range	80-90
year	2014-02
権利	(C) 2013 International Society for Photogrammetry and Remote Sensing, Inc. (ISPRS). NOTICE: this is the author's version of a work that was accepted for publication in ISPRS journal of photogrammetry and remote sensing. Changes resulting from the publishing process, such as peer review, editing, corrections, structural formatting, and other quality control mechanisms may not be reflected in this document. Changes may have been made to this work since it was submitted for publication. A definitive version was subsequently published in ISPRS journal of photogrammetry and remote sensing, 88,2014. http://dx.doi.org/10.1016/j.isprsjprs.2013.11.020
URL	http://hdl.handle.net/2241/121230

doi: 10.1016/j.isprsjprs.2013.11.020

Mapping the human footprint from satellite measurements in Japan

Fan Yang [1], Bunkei Matsushita* [1], Wei Yang [2], Takehiko Fukushima [1]

1. Graduate School of Life and Environmental Science, University of Tsukuba, 1-1-1, Tennoudai, Tsukuba, Ibaraki. 305-8572, Japan

2. State Key Laboratory of Earth Surface Processes and Resource Ecology, Beijing Normal University, Beijing 100857, China

* Corresponding Author

Tel: +81-29-853-7190

Fax: +81-29-853-7190

E-mail: matsushita.bunkei.gn@u.tsukuba.ac.jp

Mapping the human footprint from satellite measurements in Japan

Abstract

Due to increasing global urbanization and climate change, the quantification of "human footprints" has become an urgent goal in the fields of biodiversity conservation and regional environment management. A human footprint is defined as the impact of a particular human activity on the Earth's surface, which can be represented mainly by impervious surfaces (related to industry and urbanization) and cropland (related to agriculture). Here we present a method called sorted temporal mixture analysis with post-classification (STMAP) for mapping impervious surfaces and cropland simultaneously at the subpixel level to fill the demand for precise human footprint information on a national scale. The STMAP method applies a four-endmember sorted temporal mixture analysis to provide the initial fractions of evergreen forests, deciduous forests, cropland, and impervious surfaces as a first step. Endmembers are selected from the sorted temporal profiles of the MODIS-normalized difference vegetation index (NDVI), as guided by a principal component analysis. The yearly maximum land surface temperatures and averaged stable nighttime light are then statistically analyzed to provide the thresholds for post-classification to further separate cropland from deciduous forest and bare land from impervious surface. As the four outputs of STMAP, the fractions of forest, cropland, impervious surfaces and bare land are derived. We used the reference maps of impervious surfaces and cropland obtained from the Landsat/TM and ALOS precise land-use/land-cover map at the subpixel level to evaluate the performance of the proposed method, respectively. Historical satellite images with high spatial resolution were used to further evaluate the cropland results derived with the STMAP method. The

results showed that the STMAP method has promising accuracy for estimating impervious surfaces and cropland in Japan. The root mean square errors obtained with the STMAP method were 6.3% for the estimation of impervious surfaces and 9.8% for the estimation of cropland. Our findings can extend the applications of remote sensing technologies in ecological research and environment management on a large scale.

Keywords

Human footprint; impervious surface; cropland; temporal mixture analysis; MODIS; NDVI time series

1. Introduction

Two of the core issues in ecology are the conservation of biodiversity and the improvement of ecosystem services in the context of global climate change (Dawson et al., 2011). With the global population exceeding 7 billion, massive human activity has become a leading driver affecting the ecosystem. There are few studies focusing on the quantitative impact assessment of human activity as it affects biodiversity on a regional scale, although scientists have already realized the key role human activity plays in ecosystems (Loreau et al., 2001). One reason may be that the estimation of human activity on a regional scale is one of the biggest challenges that ecological scientists are facing.

Satellite remote sensing techniques, which have the inherent ability to monitor spatial and temporal information on the Earth's surface, may provide the means by which to effectively analyze the impact of human activity on ecosystems on a regional scale (Kerr and Ostrovsky, 2003). Human footprints, defined as the impressions of human activity on the Earth's surface, can be analyzed using satellite images. Previous studies on urban remote sensing and agricultural remote sensing have built a scientific basis for quantifying human footprints.

An impervious surface (or an artificial surface) is a major human footprint made on the Earth's surface during the urbanization process (Irwin and Bockstael, 2007; Sutton et al., 2009). The quantification of impervious surfaces is one of the most widely examined topics in urban remote sensing (Weng, 2012), because impervious surface coverage is not only an indicator of the degree of urbanization, but also a major indicator of the impact of urbanization on water resources and the natural ecosystem (Arnold and Gibbons, 1996; Schueler, 1994). An impervious surface generally results in spectral heterogeneity on a scale comparable to the sensors' spatial

resolution, which limits the utility of conventional hard classification methods (Small, 2001). Therefore, many unmixing methods based on spectral information have been developed to overcome this limitation.

The most typical method is the spectral mixture analysis (SMA) based on the Vegetation-Impervious-Soil (V-I-S) model (Ridd, 1995). In the V-I-S model-based SMA, there are several endmembers (pure materials) which represent the land cover type, i.e., vegetation, areas of impervious surface, and soil. Wu and Murray (2003) succeeded in extracting the impervious surface fraction by using the data for the vegetation, impervious surface (low albedo and high albedo), and soil endmembers. Lu and Weng (2006) improved this method by adding the information of land surface temperature to filter out the bare soil with high albedo. Normalization (Wu, 2004) and a multiple-endmember solution (Powell et al., 2007) were also applied to enhance the SMA method by reducing the endmember variability.

In addition to SMA, there are other solutions that were developed to estimate impervious surfaces on an urban or drainage basin scale, such as considering impervious surfaces as a complement of the vegetation distribution (e.g., Bauer et al., 2007; Carlson and Arthur, 2000), or calculating impervious surfaces using a regression approach (e.g., Elvidge et al., 2007), an artificial neural network (ANN; e.g., Weng and Hu, 2008; Hu and Weng, 2009), or an object-based image analysis (OBIA; e.g., Benz et al., 2004; Hu and Weng, 2010; Hu and Weng, 2011). More details are provided in the review by Weng (2012). However, on the national or regional scale, the methods used are still inadequate to accurately determine the amounts of impervious surface, due to the fact that low temporal resolution (16-day) and small swath width (185 km) of Landsat-style data limit the frequency of updating (Xian and Homer, 2010).

To estimate the impervious surface on a national scale, Yang et al. (2012b) developed a sorted temporal mixture analysis (STMA) by using rearranged temporal profiles of the normalized difference vegetation index (NDVI) to unmix the pixels. Similar to other methods, one remaining problem with the STMA in the Yang et al. (2012b) study was that impervious surface and bare land could not be distinguished due to the similarity between the temporal profiles of those two land cover types (Yang 2012b). On the other hand, as an advantage of STMA, the cropland fraction can also be estimated simultaneously, which extends the possible applications of STMA to the field of agricultural remote sensing.

Agriculture is one of the most important human enterprises on the Earth's surface (Vitousek et al., 1997). In remote sensing, an agricultural human footprint can be quantitatively described as cropland. The precise estimation of cropland is a central topic of agricultural remote sensing in studies of food security (Lobell et al., 2008) and the global carbon and nitrogen cycle (Robertson et al., 2000). It is difficult to quantify cropland versus other vegetation types by using Landsat-style images, because of the limitations caused by spectral similarity and low temporal resolution.

Instead, satellite images with high temporal resolution are widely used to analyze cropland spatially (Brown et al., 2012; Moran et al., 1997; Quarmby et al., 1992; Sakamoto et al., 2005), since those images can capture the identical phenology of cropland despite their low spatial resolution (250 m – 1 km). Therefore, to overcome the spatial resolution limitation of such images, researchers apply unmixing to precisely extract the fraction information of cropland at the sub-pixel level (Lobell and Asner, 2004; Oleson et al., 1995; Ozdogan, 2010).

Unfortunately, when unmixing is applied to high-temporal-resolution images on the national or regional scale, the phenological profiles of the same vegetation in

different geographic locations can shift along the time axis due to the climatic conditions. This problem was not prominent in previous studies that focused on local croplands (De Jong et al., 2011; Lobell and Asner, 2004; Oleson et al., 1995; Ozdogan, 2010; Verbesselt et al., 2010). STMA solves this problem through a sorting process (i.e., the rearrangement of NDVI temporal profiles from minimum to maximum according to the values of NDVI) and has proven to be effective to reduce the endmember variability (Yang et al., 2012b).

As a follow-up study, Yang et al. (2012a) tested the STMA to quantify the subpixel land covers by using supervised endmembers, and they reported an underestimation of cropland, caused mainly by the similarity between the temporal profiles of deciduous forest and cropland. Consequently, there remains a need for an efficient method that can precisely estimate both impervious surface and cropland, both of which represent the human footprint.

To fill the demand for precise impervious surface and cropland products on a national scale, we present an STMA with post-classification (STMAP) method for mapping remotely detectable human activities (i.e., impervious surface and cropland areas) in Japan. This method contains a four-endmember STMA model and a post-classification process that regroups the fractions to improve the accuracy. In Section 2, the required datasets are described. STMA is extended to a four-endmember model (evergreen forest, deciduous forest, cropland and impervious surface) in Section 3.1. In Section 3.2, a post-classification process using the yearly maximum land surface temperature and stable nighttime light regroups the initial fractions into forest, cropland, impervious surface and bare land at the sub-pixel level. The accuracy of the impervious surface and cropland estimates by STMAP are assessed by comparing them to the local reference data in Japan (Section 3.3). The fraction maps for

impervious surface and cropland are shown and evaluated in Section 4. In Section 5, we discuss the results and implications, and present the general conclusion of this study.

2. Data processing

There are three types of satellite images included as inputs to be examined by the new method. The first type is the NDVI temporal profile from MODIS (the Moderate Resolution Imaging Spectroradiometer), which provides temporal information about the land surface. The second is the land surface temperature (LST) from MODIS, which is used in post-classification as a filter for impervious surface and cropland. The third type of satellite image is nighttime light from DMSP-OLS (the U. S. Air Force's Defense Meteorological Satellite Program–Operational Linescan System), which is also used in post-classification as a filter for impervious surface. The final result identifying impervious surface is assessed using three reference maps of impervious surface made from Landsat images, and cropland is assessed according to the ALOS precise land-use/land-cover map (ALOS LULC map, 2013) in Japan, produced by the Earth Observation Research Center (EORC) of the Japan Aerospace Exploration Agency (JAXA).

The MODIS 16-day vegetation index (VI) products (MOD13Q1; spatial resolution: 250 m) covering the four main islands of Japan (tile numbers: h27v04, h28v04, h28v05 and h29v05; Fig. 1) in 2001, 2006, and 2011 were downloaded from NASA's Earth Observing System Data and Information System (EOSDIS). The nadir-adjusted NDVI temporal profiles (23 elements in total for one year) with pixel reliability were extracted. The NDVI temporal profiles were further smoothed to improve the data quality by using a Savitzky-Golay filter-based method (Chen et al.,

2004). This method is based on the assumptions that the NDVI temporal profiles follow the phenology of vegetation, and that clouds or poor atmospheric conditions usually depress NDVI values. This method has been proved to be effective to smooth out noise in NDVI temporal profiles, specifically the noise caused by cloud contamination and atmospheric variability (Chen et al., 2004).

There are two main parameters used in the Savitzky-Golay filter: one is the degree of the polynomial function (d), and the other is the local window size for the smoothing calculation (w). In this study, the default values of d=3 and w=4 were used. The yearly maximum LST values were calculated from MODIS 8-day LST measurements (MOD11A2; spatial resolution: 1 km) in 2001, 2006 and 2011. Three images of averaged stable DMSP-OLS nighttime light in 2001, 2006, and 2010 (F152001, F162006 and F182010; spatial resolution: 1 km) were downloaded from the National Geophysical Data Center (NGDC) of the U.S. National Oceanic and Atmospheric Administration (NOAA). The yearly maximum LST values and averaged stable nighttime light were resampled (using the nearest neighbor method) to 250 m to match the spatial resolution of the NDVI temporal profiles.

To determine the thresholds of LST and nighttime light for cropland, we used the national actual vegetation map (published by the Natural Conservation Bureau of the Ministry of the Environment of Japan, based on the latest National Survey on the Natural Environment (the Green Census), conducted from 1993 to 1998) to obtain detailed information about local vegetation types in Japan. To fit the needs of this study, the actual national vegetation map was reclassified into 10 classes: alpine scrub/snow patch (0.3%), subalpine needle leaf forest (5.1%), evergreen needle leaf forest (22.5%), deciduous needle leaf forest (3.7%), evergreen broadleaf forest (25.6%), deciduous broadleaf forest (16.7%), wetland (0.4%), grassland (3.0%),

bamboo (0.1%) and crop field (16.5%). The percentages in parentheses are the total coverage. After excluding the roads and buildings (using a map provided by the Geospatial Information Authority of Japan), this modified vegetation map was converted from vector to raster format (using the area prior method) with a spatial resolution of 250 m.

Three Landsat-5 TM images covering Sapporo City (Hokkaido Prefecture, North Japan) on July 31, 2007, the Kanto Plain (East Japan) on July 11, 2000 and central Kagoshima Prefecture (Southwest Japan) on February 13, 2000 (Fig. 1) were used to generate the reference impervious surface fraction map for accuracy assessment. The impervious surface fraction was generated by the pre-screened and normalized multiple endmember spectral mixture analysis (PNMESMA) method (Yang et al., 2010). In the PNMESMA method, pre-screening of pure vegetation pixels, the normalization process and multiple endmember solutions are combined to reduce the endmember variability and improve the accuracy. Validation by using aerial photographs (with a spatial resolution of 0.5 m) proved that the estimation error of PNMESMA is 5.2%, and no obvious underestimation or overestimation occurs (Yang et al., 2010).

The reference fraction maps of impervious surface in 2000 (Kanto Plain and Kagoshima Prefecture) and 2007 (Hokkaido Prefecture) were used to assess those fraction maps from MODIS in 2001 and 2006, respectively. This is because Landsat images were not available for 2001 and 2006 in our study areas. The land use/cover changes between 2000 and 2001 as well as 2006 and 2007 are ignored.

A reference fraction map of cropland was generated from an ALOS LULC map. The ALOS LULC map was produced by using multi-temporal ALOS/AVNIR-2 images with auxiliary data such as a digital elevation model, ALOS/PALSAR images,

Terra/MODIS NDVI time series and road maps in Japan. It has a spatial resolution of 50 m, and has nine classes (water, urban area, paddy field, plowed field, grass, deciduous forest, evergreen forest, bare land, snow/ice). The total accuracy of the ALOS LULC map is 88.1% compared to the statistical data that provide the total coverage of the current land use for each prefecture of Japan (published by the Ministry of Internal Affairs and Communications [MIC] in 2009). The current version (ver.12.08) was downloaded, and the classes of paddy field and plowed field were merged as cropland with a user accuracy of 87.5% (assessed using approx. 2500 random samples in Japan). Reference fraction maps of impervious surface and cropland were re-sampled (pixel-aggregated) to 250 m to match the spatial resolution of the NDVI temporal profiles.

3. Methodology

3.1. Development of a four-endmember sorted temporal mixture analysis

Temporal mixture analysis (TMA), which is algebraically identical to spectral mixture analysis (SMA) but uses temporal profiles instead of electromagnetic spectra, is another mixture analysis technique to estimate the fraction of each endmember based on the different temporal characteristics of the endmembers (Piwowar et al., 1998). For a given pixel, a temporal profile (ρ_{mix}) can be unmixed by using a constrained linear mixture model as follows:

$$NDVI_{mix} = \sum_{i=1}^{N} f_i \times NDVI_i + \varepsilon \quad (1)$$

$$\sum_{i=1}^{N} f_i = 1, \; f_i \geq 0 \quad (2)$$

where $NDVI_{mix}$ is the temporal profile of the NDVI of the target pixel, $NDVI_i$ is the temporal profile of the NDVI of endmember i, f_i is the fraction of endmember i, and ε is the residual representing the model error. In this study, the fraction of each

endmember was obtained using the constrained_min function in IDL 5.0 (Interactive Data Language; Exelis Visual Information Solutions Inc., Boulder, CO).

To reduce the endmember variability in TMA, Yang et al. (2012b) proposed the use of a sorted NDVI temporal profile (i.e., rearranging the NDVI temporal profiles from minimum to maximum according to the NDVI values) instead of the original one. The variability of NDVI temporal profiles within each vegetation endmember could be greatly reduced through the sorting process. This is because the NDVI temporal profiles within the same vegetation endmember have similar shapes but different time phases due to the different climatic conditions in different regions of Japan.

In addition, Yang et al. (2012b) found that the standard deviations in the high-NDVI zone are significantly smaller than those in the low-NDVI zone for all vegetation types, and thus NDVI temporal profiles in the high-NDVI zone have the potential to be summarized as an endmember with low variability. Therefore, the last six maximum NDVI values in the sorted NDVI temporal profiles were selected to further reduce endmember variability (Yang et al., 2012b). To distinguish between the use of the original and sorted NDVI temporal profiles in the TMA, the latter was called STMA (sorted temporal mixture analysis) in the present study. Details of the STMA can be found in Yang et al. (2012b).

Compared to the previous version of STMA in Yang et al. (2012b), two improvements were made in the present study. First, the analysis period was extended from the last six maximum NDVI values to the last 12 maximum NDVI values in a sorted temporal profile. This improvement allows the separation of deciduous forest from evergreen forest by using their different temporal characteristics. Second, the number of endmembers was increased from three (forest, cropland, and impervious

surface) to four (evergreen forest, deciduous forest, cropland, and impervious surface) based on the first improvement. The separation of deciduous forest from evergreen forest was done because some cropland and deciduous forests were often misestimated as the other and thus further refinements were necessary (Yang et al., 2012a).

We carried out a principal component analysis (PCA) for the last 12 maximum NDVI values in sorted NDVI temporal profiles to guide endmember selection in the image. Figure 2 shows the feature spaces of the first three principal components (PCs) representing 99.6% of the variance in the sorted NDVI temporal image. Four endmembers were identified in the feature spaces of PC1 versus PC2 (Fig. 2a) and PC1 versus PC3 (Fig. 2b), respectively.

The temporal profiles of selected endmembers are shown in Figure 3. It can be seen that even when the NDVI temporal profiles were sorted, the phenological characteristic of each endmember could still be maintained. For example, the NDVI temporal profile of cropland showed a slowly increasing trend compared to that of deciduous forest even in the high-NDVI zone, whereas the NDVI temporal profiles of the evergreen forests and impervious surface showed almost no change in the high-NDVI zone. The initial fraction information for any given pixel is calculated by Eq. 1 using the constraints of Eq. 2.

3.2. Post-classification

According to our previous work (Yang et al., 2012a), due to the similar NDVI temporal profiles between bare land (e.g., soil, rock, desert, etc.) and impervious surface as well as between cropland (due mainly to the plowed field) and deciduous forest, some estimation errors will occur if only the STMA was used to estimate the

fractions of impervious surface and cropland. Therefore, a post-classification approach is needed to further reduce the estimating errors between cropland and deciduous forest and between impervious surface and bare land.

In the post-classification, two additional datasets that are widely used in human activity-related researches were employed. The first is the LST. Nemani and Running (1997) reported that cropland can be effectively separated from forest based on the yearly maximum LST, since the higher aerodynamic resistances of crops suppress detectable heat transfer, resulting in higher LSTs. The second dataset is the nighttime light, which is used to filter bare land from the impervious surface fraction. Nighttime light can be used to monitor human settlements (Croft, 1973) and impervious surfaces (Elvidge et al., 2007) based on the fact that most of the nighttime lights are from human settlements (Elvidge et al., 1999).

The threshold selections for post-classification were based on the statistical analysis results (Figs. 4, 5). A vegetation map published by the Natural Conservation Bureau of the Ministry of the Environment of Japan (described in Section 2) was used to assist with the statistical analysis. The values (from lower to upper limit, 5%, 25%, 50%, 75%, and 95%) of LST and nighttime light for the 10 main vegetation types in Japan are shown in Figures 4 and 5, respectively. We selected the value of yearly maximum LST for cropland for the 5th percentile (i.e., 299 K) as the threshold to correct estimation errors in cropland; that is, if a pixel was estimated with a non-zero fraction of cropland but the yearly maximum LST was less than 299 K, the estimated cropland fraction should be modified as the fraction of forest, and the cropland fractions should be reset as zero.

This is because only a few cropland pixels with a yearly maximum LST smaller than 299 K can be found from Figure 4. We selected another value of yearly

maximum LST for deciduous forest for the 95th percentile (i.e., 304 K) as the threshold to correct the estimation errors in deciduous forest; that is, if a pixel was estimated with a non-zero fraction of deciduous forest but the yearly maximum LST was larger than 304 K, the estimated fraction of deciduous forest should be modified as the fraction of cropland, and the fraction of deciduous forest should be reset as zero. This is because only a few forest pixels with a yearly maximum LST larger than 304 K can be found from Figure 4. However, we found that if the yearly maximum LST exceeded 310 K, the impervious surface area (ISA) was the dominant component of the pixel, and then it was difficult to regroup the deciduous forest and cropland in this pixel. Therefore, the modification between deciduous forest and cropland should not be carried out if the yearly maximum LST is larger than 310 K.

Since the NDVI temporal profiles were used in the mixture analysis in this study, it is difficult or impossible to separate bare land from impervious surface, and thus the analysis sometimes results in a slight overestimation of the ISA. To address this problem, we used the yearly averaged nighttime light data. It is assumed that if a pixel has a larger estimated ISA fraction but lower yearly averaged nighttime light, the estimated ISA fraction should be modified as the fraction of bare land, and the ISA fraction should be reset as zero.

From Figure 5, it can be seen that the digital numbers (DNs) of the yearly averaged nighttime light in vegetation areas are almost all smaller than 15. The few exceptions, especially in cropland, probably arise because these pixels are in or close to urban areas. In addition, by examining the estimated ISA fraction around Mount Fuji, we found that all of the investigated pixels had an estimated ISA fraction larger than 30%. We therefore selected the threshold of the ISA fraction as 30% and that of

the DN of yearly averaged nighttime light as 15 to correct the estimation errors in the ISA fraction.

Figure 6 is the flowchart of the STMAP method. Four endmembers (evergreen forest, deciduous forest, cropland and impervious surface) are selected from the sorted NDVI time series, guided by a principal component analysis. The initial fraction of each endmember is calculated via a sorted temporal mixture analysis. With the threshold values determined by yearly maximum LSTs and averaged stable nighttime light, the post-classification is conducted in four steps: (1) if the LST is smaller than 299 K, the fractions of evergreen forest, deciduous forest, and cropland are merged to be that of forest, and the impervious surface fraction is classified as that of bare land; (2) if the LST is between 304 and 310 K, the fraction of evergreen forest is classified as that of forest, and deciduous forest and cropland are merged as cropland, and impervious surface is kept as it is; (3) if the DN of nighttime light is not larger than 15 but the impervious surface fraction is not smaller than 30%, the fractions of evergreen forest and deciduous forest are merged to be that of forest, the cropland is kept as-is, and impervious surface is classified as bare land; (4) otherwise, the fractions of evergreen forest and deciduous forest are merged to be that of forest, and cropland and impervious surface are maintained as-is. After the post-classification, four final fractional results—i.e., the results for forest, cropland, impervious surface, and bare land—are determined.

3.3. Accuracy assessment

We assessed the accuracy of the STMAP method by comparing its results to the reference maps of the Kanto Plain, Sapporo City, and central Kagoshima Prefecture. These three areas were chosen because Tokyo is the largest city in the Kanto Plain,

and Sapporo is the largest city in northern Japan, and each city has large areas of surrounding cropland. Kagoshima City in central Kagoshima Prefecture is a relatively small city surrounded by a rural area in southwestern Japan.

First, each reference map and corresponding fraction map estimated from MODIS data were evenly segmented into 10 × 10 meshes; a sampling window with a size of 1 km × 1 km at the center of each mesh was then extracted for the accuracy assessment. Therefore, a total of 100 samples was obtained for each place (i.e., Kanto Plain, Sapporo City, and Kagoshima City). After excluding the sampling windows that probably included a small water area or cloud contamination, there were 33, 68, and 36 sampling windows left for assessing the impervious surface in central Kagoshima Prefecture, the Kanto Plain, and Sapporo City, respectively. A 1 km × 1 km sampling unit (4 × 4 MODIS pixels) was used to reduce the geometric correction errors associated with the different data sources.

Three types of error measurement, i.e., root mean square error (RMSE) (Eq. 3), systematic error (SE) (Eq. 4), and mean absolute error (MAE) (Eq. 5), were employed to evaluate the accuracy of STMAP:

$$RMSE = \sqrt{\sum_{j=1}^{M} (X_{est,j} - X_{ref,j})^2 / M} \tag{3}$$

$$SE = \sum_{j=1}^{M} (X_{est,j} - X_{ref,j}) / M \tag{4}$$

$$MAE = \sum_{j=1}^{M} \left| X_{est,j} - X_{ref,j} \right| / M \tag{5}$$

where $X_{est,j}$ is the estimated fraction of the impervious surface or cropland from the MODIS data and $X_{ref,j}$ is the referenced data in the sampling window j. M is the

number of sampling windows for validation (a total of 137 for the impervious surface and 300 for cropland).

4. Results

The STMAP method quantified the subpixel fractions of forest, cropland, impervious surface, and bare land. Figure 7a shows the spatial distribution map of the impervious surface, which represents urban human footprints in Japan. The largest 10 cities ranked by the population data in 2010 (published by the Statistics Bureau, MIC) are marked. A large fraction of impervious surface is distributed mainly in large cities; a medium fraction of impervious surface is found in small cities and rural areas; and forest area, the largest land cover type in Japan, has an extremely low or no fraction of impervious surface.

The fraction map of cropland estimated in this study, which represents agricultural human footprints, is shown in Figure 7b, with the top 12 prefectures having the largest cropland (published by the Statistics Bureau, MIC in 2010). A high fraction of cropland is distributed mainly in northern and eastern Japan, where more paddy fields and plowed fields are located than in southern and western Japan; a medium fraction of cropland is found in the rural area, along with a medium fraction of impervious surface. There is a low or no fraction of cropland in large cities or forested areas. These results suggest that the STMAP method correctly captured the spatial distribution of remotely sensible human footprints visually.

We assessed the accuracy of the STMAP method by comparing its results to reference maps of impervious surface and cropland, respectively. Figure 8a is the accuracy assessment of impervious surface estimated by STMAP. The Kanto Plain and Sapporo City have more assessment windows with high impervious surface

coverage than central Kagoshima Prefecture because of the comprehensive urbanization. The estimate of impervious surface by STMAP has no obvious underestimation or overestimation in any of these three locations, and the RMSE is 0.063 in total.

Figure 8b shows the accuracy assessment of the cropland made by using the ALOS LULC map as a reference. Since there is a lot of forest area coverage in the rural areas of central Kagoshima Prefecture, the assessment windows with high cropland coverage are fewer than those in the Kanto Plain and Sapporo City. The RMSE of cropland estimated by STMAP was 0.121 in total, which is larger than that of impervious surface. This might have been caused by the spatial resolution limitation of the ALOS LULC map, whose spatial resolution is 50 m.

To analyze the error of the ALOS LULC map, we compared three different assessment datasets (Fig. 9). Figure 9a–c shows high-spatial-resolution images from Google Earth covering three assessment windows (1 km × 1 km) in Sapporo (June 12, 2012), Kanto (May 29, 2009) and Kagoshima (March 27, 2012); the estimated results of %impervious are 16.9%, 23.2% and 13.9%, and those of %cropland are 44.2%, 68.9%, and 2.6%. By checking historical records in Google Earth, it is found that no land cover change occurred in these three assessment windows from 2001 to 2012. Figure 9d–f shows the reference maps of the fractional impervious surface made from Landsat images for these three windows, and the referenced %impervious values are 21.3%, 23.4% and 11.2%, respectively. These reference maps made from Landsat images capture the distribution of impervious surface accurately at the subpixel level.

Figure 9g–i shows the ALOS LULC maps for these three sites. Pixels in blue are classified as cropland, and pixels in red are classified as urban area. Compared to the reference map of impervious surface, the ALOS LULC map has an inherent error

when assessing the cropland at the subpixel level, since it is a pixel-based classification. Another reason for the errors might be that the accuracy of the cropland designation in the ALOS LULC map depends on the available images of the ALOS AVNIR-2, whose repeat cycle is 46 days. This causes errors wherever insufficient temporal images are obtained (for example, cropland was underestimated in Fig. 9g).

We also interpreted historical images in Google Earth as a true ground reference to assess the cropland estimate by the STMAP method. We extracted 25 assessment windows that appeared to have overestimated, underestimated or well-estimated the cropland (filled points in Fig. 8b) for photo interpretation. Figure 10a is the result of the assessment for the ALOS LULC map; the RMSE was 0.128 and the SE was −0.029 in the assessment by photo interpretation. Figure 10b is the result of the assessment for the STMAP method, and the RMSE was reduced to 0.098 from 0.173 (RMSE of filled points in Fig. 8b) in the assessment by photo interpretation. This result confirmed that the error in the accuracy assessment of cropland was partly due to the inherent error of the ALOS LULC map. Although flaws exist in the ALOS LULC map, it is the only accessible spatial dataset covering all of Japan with both high spatial resolution (50 m) and frequency of updating (half a year) to assess cropland spatially in Japan.

5. Discussion

5.1. Advantages of STMA

Yang et al. (2012b) noted that the STMA has three advantages: (1) it reduces endmember variability through the sorting process; (2) cropland can be distinguished from forest with the use of the temporal characteristics; (3) investigations of the human footprint on a large scale over a long term are made possible. Endmember

variability is the most profound source of error in mixture analysis (Somers et al., 2011). In the STMA, sorting NDVI temporal profiles according to their values reduced the effects due to different vegetation phonologies under different meteorological conditions (Figs. 2 and 3 in Yang et al., 2012b), and thus small endmember variability was obtainable, especially in temporal zones with larger NDVI values (i.e., stable temporal zones, Table 1 in Yang et al., 2012b).

On the other hand, the sorting process has a demerit; that is, it unnecessarily enhances collinearity among the endmembers. The degree of correlation among the endmembers will strongly relate to the outcome of the unmixing process in terms of the error and difference between true and estimated fractions (Van der Meer and De Jong, 2000). From Figure 3, it can be seen that there are very high correlations among the four endmembers. The variance inflation factors (VIFs) were calculated as 468, 64, 59, and 764 for evergreen forest, deciduous forest, cropland, and impervious surface, respectively. As a rule of thumb, the user should start to become suspicious of the results for a VIF larger than 10 (Van der Meer and Jia, 2012).

However, to further consider the merits and the demerits of the sorting process, another metric referred to as the InStability Index (ISI; Somers et al., 2010) was used. The ISI is defined as the ratio of the within-class endmember variability to the between-class endmember variability. The accuracy of a subpixel fraction estimate decreases linearly with increasing variability within endmember classes, and it increases linearly with increasing variability among endmembers (Van der Meer and Jia, 2012).

Table 1 shows the ISI values for a two-endmember scenario in each period. It can be seen that all ISI values are smaller than 1 except for the two-endmember scenario of evergreen forest and deciduous forest. This finding indicates that the

sorting process can not only effectively reduce variability within each endmember, but also maintain the temporal characteristic of each endmember. Therefore, it can be considered that the merit derived from the sorting process is larger than the demerit derived from the same process, and thus the method provides acceptable accuracies for estimating the fractions of impervious surface and cropland.

It can also be considered that errors probably occurred in the fraction estimations between evergreen forest and deciduous forest because the ISI values were larger than 1 for several periods (Table 1). However, these errors will not affect the fraction estimations for impervious surface and cropland, because evergreen forest and deciduous forest were finally merged into one forest category (Fig. 6).

5.2. Necessity of post-classification

Table 2 shows the effects of different steps in post-classification. The first step uses LST (i.e., LST < 299 K) to remove overestimations of the fractions of impervious surface and cropland, and doing so improves the results slightly (the RMSE is reduced from 0.065 to 0.063 and the MAE is reduced from 0.034 to 0.033) for the estimation of impervious surface. The second step uses LST (i.e., LST ≥ 304 K and LST ≤ 310 K) to add the mis-estimated deciduous forest back to cropland, and doing so reduces the RMSE for estimating cropland from 0.132 to 0.122, and from 0.176 to 0.098 (Fig. 10) for the results assessed by the ALOS LULC map and photo interpretation, respectively.

The third step uses nighttime light to remove the bare land from impervious surface, and that seems to have had little effect on the three assessment areas. As detailed in Table 2, the second step improves the results of STMA significantly, which is consistent with the findings reported by Nemani and Running (1997) in that

LST is a critical factor to separate cropland and forest, in addition to the NDVI temporal profile. The first and third steps do not cause any obvious improvement, which is consistent with the assumption (Yang et al., 2012b) that little bare land exists in Japan.

However, for applying the STMAP method to areas that include large regions of bare soil or desert, the improvements will be obvious. The overestimation or underestimation of the fraction estimations of impervious surface and cropland is due to the similar NDVI temporal profiles between impervious surface and bare land, as well as some cropland and deciduous forest. Therefore, the post-classification is necessary to further refine the results of fraction estimations by STMA.

5.3. Limitations and recommendations of the proposed method

Some limitations of the STMAP method are worth noting. The method is based on images derived by optical sensors, and thus the impact of weather conditions should be considered. Although the filtering and sorting process guarantees the quality of temporal data, it still might be difficult to apply the system in some countries with a low ratio of good-weather days. In this case, the solution of applying radar data (e.g., Lu et al., 2011) could be an alternative. Another limitation of the STMPA method is the thresholds used in the process of post-classification. Although the statistical thresholds in this study are close to the global thresholds (Nemani and Running, 1997), we suggest a local investigation before performing the STMAP method if land cover/use data are available.

In the present study, cropland was not further classified as paddy fields and plowed fields, since these fields represent agricultural human footprints. The role of paddy fields is especially important in the dynamic analyses of nutrition with regard

to water quality (Fukushima et al., 2007), because of the unique farming process involved. As a future application, we plan to distinguish paddy fields from other cropland by classifying the water use at the subpixel level with high accuracy. In addition, to quantify the impact of human activity on a regional environment or ecosystem, we must determine how to integrate the effects of urban and agricultural human footprints into the process of environment and ecosystem assessments.

6. Conclusions

Here we proposed a sorted temporal mixture analysis with a post-classification (STMAP) method to simultaneously estimate the fractions of impervious surface and cropland, which represent the human footprints on the Earth's surface. In the STMAP method, the initial fractions of impervious surface and cropland were calculated from MODIS time-series NDVI using the sorted temporal mixture analysis (STMA) method, and then the initial results were improved through a post-classification based on the information of land surface temperature (LST) from MODIS and nighttime light from DMSP-OLS. Three datasets (i.e., the fraction of impervious surface from Landsat/TM, the cropland fraction from the ALOS LULC map, and the cropland fraction from a Google Earth map) were used to validate the performance of the proposed method. The results showed that the STMAP method has promising accuracy for estimating the fractions of impervious surface and cropland in Japan. The RMSEs were 6.3% for the estimation of impervious surface and 9.8% for the estimation of cropland. The fractions of impervious surface and cropland on the national scale can be further applied to the impact assessment of human activities on biodiversity and regional environment management. The results of this study can be

expected to broaden the applications of remote sensing technology in ecological research and environment management.

Acknowledgements

This study was supported by the Environment Research and Technology Development Fund (S-9-4-(1)) of the Ministry of the Environment, Japan and Grants-in-Aid for Scientific Research of MEXT, Japan (No.21241001, No. 21401001, and No. 25420555). The valuable comments from reviewers improved the scientific level of this paper. The authors are indebted to Dr. ISHITSUKA Naoki at National Institute for Agro-Environmental Sciences (NIAES), Associate Professor NASAHARA N. Kenlo at University of Tsukuba for the valuable discussion on an earlier draft. Special thanks should be given to Ms. IGUCHI Rie and Mr. SHINOHARA Takayuki for the efficient assistant in data collection and data processing.

Reference

Arnold, C. L., Gibbons, C. J., 1996. Impervious surface coverage: the emergence of a key environmental indicator. Journal of the American Planning Association 62(2), 243–258.

ALOS LULC map, 2013. ALOS precise land-use/land-cover map (ALOS LULC map) of Japan, produced by the Earth Observation Research Center (EORC), Japan Aerospace Exploration Agency (JAXA). < http://www.eorc.jaxa.jp/ALOS/lulc/lulc_jindex.htm> (accessed January 4, 2013).

Bauer, M. E., Loffelholz, B. C., Wilson, B., 2007. Estimating and mapping impervious surface area by regression analysis of Landsat imagery. In Q. Weng (Ed.), Remote Sensing of Impervious Surfaces (pp. 3-19). Boca Raton, Florida: CRC Press.

Benz, U. C., Hofmann, P., Willhauck, G., Lingenfelder, I., Heynen, M., 2004. Multi-resolution, object-oriented fuzzy analysis of remote sensing data for GIS-ready information. ISPRS Journal of Photogrammetry and Remote Sensing 58, 239-258.

Brown, M. E., De Beurs, K. M., Marshall, M., 2012. Global phenological response to climate change in crop areas using satellite remote sensing of vegetation, humidity and temperature over 26 years. Remote Sensing of Environment 126, 174–183.

Carlson, T. N., Arthur, S. T., 2000. The impact of land use-land cover changes due to urbanization on surface microclimate and hydrology: A satellite perspective. Global and Planetary Change 25, 49-65.

Chen, J., Jönsson, P., Tamura, M., Gu, Z., Matsushita, B., Eklundh, L., 2004. A simple method for reconstructing a high-quality NDVI time-series data set based on the Savitzky-Golay filter. Remote Sensing of Environment 91(3-4), 332–344.

Croft, T.A., 1973. Burning Waste Gas in Oil Fields. Nature 245, 375–376

Dawson, T. P., Jackson, S. T., House, J. I., Prentice, I. C., Mace, G. M., 2011. Beyond predictions: biodiversity conservation in a changing climate. Science 332(6025), 53–8.

De Jong, R., De Bruin, S., De Wit, A., Schaepman, M. E., Dent, D. L., 2011. Analysis of monotonic greening and browning trends from global NDVI time-series. Remote Sensing of Environment 115(2), 692–702.

Elvidge, C.D., Baugh, K. E., Dietz, J. B., Bland, T., Sutton, P. C., Kroehl, H. W., 1999. Radiance calibration of DMSP-OLS low-light imaging data of human settlements. Remote Sensing of Environment 68(1), 77–88.

Elvidge, Christopher D., Tuttle, B. T., Sutton, P. C., Baugh, K. E., Howard, A. T., Milesi, C., Bhaduri, B., Nemani, R., 2007. Global distribution and density of constructed impervious surfaces. Sensors 7(9), 1962–1979.

Fukushima, T., Takahashi, M., Matsushita, B., Okanishi, Y., 2007. Land use/cover change and its drivers: a case in the watershed of Lake Kasumigaura, Japan. Landscape and Ecological Engineering 3(1), 21–31.

Hu, X., Weng, Q., 2009. Estimating impervious surfaces from medium spatial resolution imagery using the self-organizing map and multi-layer perceptron neural networks. Remote Sensing of Environment 113, 2089-2102.

Hu, X., Weng, Q., 2010. Impervious surface area extraction from IKONOS imagery using an object-based fuzzy method. Geocarto International 26, 3-20.

Hu, X., Weng, Q., 2011. Estimating impervious surfaces from medium spatial resolution imagery: a comparison between fuzzy classification and LSMA. International Journal of Remote Sensing 32, 5645-5663.

Irwin, E. G., Bockstael, N. E., 2007. The evolution of urban sprawl: evidence of spatial heterogeneity and increasing land fragmentation. Proceedings of the National Academy of Sciences of the United States of America 104(52), 20672–20677.

Kerr, J. T., Ostrovsky, M., 2003. From space to species: ecological applications for remote sensing. Trends in Ecology & Evolution 18(6), 299–305.

Lobell, D. B., Asner, G. P., 2004. Cropland distributions from temporal unmixing of MODIS data. Remote Sensing of Environment 93(3), 412–422.

Lobell, D. B., Burke, M. B., Tebaldi, C., Mastrandrea, M. D., Falcon, W. P., Naylor, R. L., 2008. Prioritizing climate change adaptation needs for food security in 2030. Science 319(5863), 607–610.

Loreau, M., Naeem, S., Inchausti, P., Bengtsson, J., Grime, J. P., Hector, A., Hooper, D. U., Huston M.A., 2001. Biodiversity and ecosystem functioning: current knowledge and future challenges. Science 294(5543), 804–808.

Lu, D., Li, G., Moran, E., Batistella, M., Freitas, C. C., 2011. Mapping impervious surfaces with the integrated use of Landsat Thematic Mapper and radar data: A case study in an urban–rural landscape in the Brazilian Amazon. ISPRS Journal of Photogrammetry and Remote Sensing 66(6), 798–808.

Lu, D., Weng, Q., 2006. Use of impervious surface in urban land-use classification. Remote Sensing of Environment 102(1-2), 146–160.

Moran, M. S., Inoue, Y., Barnes, E. M., 1997. Opportunities and limitations for image-based remote sensing in precision crop management. Remote Sensing of Environment 61(3), 319–346.

Nemani, R., Running, S., 1997. Land cover characterization using multitemporal red, near-IR, and thermal-IR data from NOAA/AVHRR. Ecological Applications 7(1), 79–90.

Oleson, K. W., Sarlin, S., Garrison, J., Smith, S., Privette, J. L., Emery, W. J., 1995. Unmixing multiple land-cover type reflectances from coarse spatial resolution satellite data. Remote Sensing of Environment 54(2), 98–112.

Ozdogan, M., 2010. The spatial distribution of crop types from MODIS data: Temporal unmixing using Independent Component Analysis. Remote Sensing of Environment 114(6), 1190–1204.

Piwowar, J. M., Peddle, D. R., LeDrew, E. F., 1998. Temporal mixture analysis of arctic sea ice imagery: a new approach for monitoring environmental change. Remote Sensing of Environment 63(3), 195–207.

Powell, R. L., Roberts, D. A., Dennison, P. E., Hess, L. L., 2007. Sub-pixel mapping of urban land cover using multiple endmember spectral mixture analysis: Manaus, Brazil. Remote Sensing of Environment 106(2), 253–267.

Quarmby, N. A., Townshend, J. R. G., Settle, J. J., White, K. H., Milnes, M., Hindle, T. L., Silleos, N., 1992. Linear mixture modelling applied to AVHRR data for crop area estimation. International Journal of Remote Sensing 13, 415–425

Ridd, M. K., 1995. Exploring a V-I-S (vegetation-impervious surface-soil) model for urban ecosystem analysis through remote sensing: comparative anatomy for cities. International Journal of Remote Sensing 16(12), 2165–2185.

Robertson, G. P., Paul, E. A., Harwood, R. R., 2000. Greenhouse Gases in Intensive Agriculture: Contributions of Individual Gases to the Radiative Forcing of the Atmosphere. Science 289(5486), 1922–1925.

Sakamoto, T., Yokozawa, M., Toritani, H., Shibayama, M., Ishitsuka, N., Ohno, H., 2005. A crop phenology detection method using time-series MODIS data. Remote Sensing of Environment 96(3-4), 366–374.

Schueler, T. R., 1994. The Importance of Imperviousness. Watershed Protection Techniques 1(3), 100–111.

Small, C., 2001. Estimation of urban vegetation abundance by spectral mixture analysis. International journal of remote sensing 22(7), 1305–1334.

Somers, B., Asner, G. P., Tits, L., Coppin, P., 2011. Endmember variability in Spectral Mixture Analysis: A review. Remote Sensing of Environment 115(7), 1603–1616.

Somers, B., Delalieux, S., Verstraeten, W.W., Van Aardt, J.A.N., Albrigo, G.L., Coppin, P., 2010. An automated waveband selection technique for optimized hyperspectral mixture analysis. International Journal of Remote Sensing 31(20), 5549-5568.

Sutton, P. C., Anderson, S. J., Elvidge, C. D., Tuttle, B. T., Ghosh, T., 2009. Paving the planet: impervious surface as proxy measure of the human ecological footprint. Progress in Physical Geography 33(4), 510–527.

Van der Meer, F.D., De Jong, S.M., 2000. Improving the results of spectral unmixing of LANDSAT thematic mapper imagery by enhancing the orthogonality of end - members. International journal of remote sensing 21(15), 2781-2797.

Van der Meer, F.D., Jia, X.P., 2012. Collinearity and orthogonality of endmembers in linear spectral unmixing. International Journal of Applied Earth Observation and Geoinformation 18, 491-503.

Verbesselt, J., Hyndman, R., Newnham, G., Culvenor, D., 2010. Detecting trend and seasonal changes in satellite image time series. Remote Sensing of Environment 114(1), 106–115.

Vitousek, P. M., Mooney, H. A., Lubchenoco, J., Melillo, J. M., 1997. Human Domination of Earth's Ecosystems. Science 277(5325), 494–499.

Weng, Q., Hu, X., 2008. Medium spatial resolution satellite imagery for estimating and mapping urban impervious surfaces using LSMA and ANN. IEEE Transactions on Geoscience and Remote Sensing 46, 2397-2406.

Weng, Q., 2012. Remote sensing of impervious surfaces in the urban areas: Requirements, methods, and trends. Remote Sensing of Environment 117(2), 34–49.

Wu, C., 2004. Normalized spectral mixture analysis for monitoring urban composition using ETM+ imagery. Remote Sensing of Environment 93(4), 480–492.

Wu, C., Murray, A. T., 2003. Estimating impervious surface distribution by spectral mixture analysis. Remote Sensing of Environment 84(4), 493–505.

Xian, G., Homer, C., 2010. Updating the 2001 National Land Cover Database Impervious Surface Products to 2006 using Landsat Imagery Change Detection Methods. Remote Sensing of Environment 114(8), 1676–1686.

Yang, F., Matsushita, B., Fukushima, T., 2010. A pre-screened and normalized multiple endmember spectral mixture analysis for mapping impervious surface area in Lake Kasumigaura Basin, Japan. ISPRS Journal of Photogrammetry and Remote Sensing 65(5), 479–490.

Yang, F., Matsushita, B., Fukushima, T., 2012a. Testing temporal mixture analysis for quantification of land cover at sub-pixel level. Proceedings of the 2nd International Workshop on Earth Observation and Remote Sensing Applications, EORSA 2012 (pp. 50–54). IEEE Xplore.

Yang, F., Matsushita, B., Fukushima, T., Yang, W., 2012b. Temporal mixture analysis for estimating impervious surface area from multi-temporal MODIS NDVI data in Japan. ISPRS Journal of Photogrammetry and Remote Sensing 72, 90–98.

Tables and Figures

Table 1. InStability Index calculation for a two endmember scenario in each period.

Period No.	E-D	E-C	E-I	D-C	D-I	C-I
12	0.257	0.118	0.077	0.159	0.454	0.445
13	0.462	0.119	0.075	0.162	0.371	0.406
14	0.468	0.122	0.074	0.113	0.233	0.373
15	0.912	0.134	0.074	0.106	0.204	0.325
16	1.477	0.160	0.074	0.083	0.149	0.278
17	6.293	0.192	0.075	0.076	0.136	0.238
18	9.691	0.229	0.075	0.067	0.124	0.197
19	5.716	0.308	0.076	0.064	0.119	0.179
20	6.412	0.340	0.074	0.055	0.115	0.143
21	9.392	0.438	0.073	0.050	0.109	0.133
22	10.558	0.473	0.074	0.042	0.105	0.115
23	6.524	0.537	0.075	0.041	0.104	0.113
average	4.847	0.264	0.075	0.085	0.185	0.246

E: evergreen forest, D: deciduous forest, C: cropland, I: impervious surface

Table 2 Comparisons of the estimation accuracies of impervious surface and cropland among different methods

Method	Impervious			Cropland		
	RMSE	SE	MAE	RMSE	SE	MAE
STMA	0.065	0.015	0.034	0.132	-0.033	0.085
STMA + 1st step	0.063	0.015	0.033	0.132	-0.034	0.084
STMA + 2nd step	0.065	0.015	0.034	0.122	0.026	0.084
STMA + 3rd step	0.065	0.015	0.034	0.132	-0.033	0.085
STMAP	0.063	0.014	0.033	0.122	0.025	0.083

STMA: sorted temporal mixture analysis

STMA + 1st step: STMA with the first step of post-classification process (i.e. LST<299K in Fig. 6)

STMA + 2nd step: STMA with the second step of post-classification process (i.e. LST≥304K and LST≤310K in Fig. 6)

STMA + 3rd step: STMA with the third step of post-classification process (i.e. $DN_{light}\leq 15$ and $f_{imp,0}\geq 30\%$ in Fig. 6)

STMAP: STMA with whole post-classification process

RMSE: root mean square error

SE: system error

MAE: mean absolute error

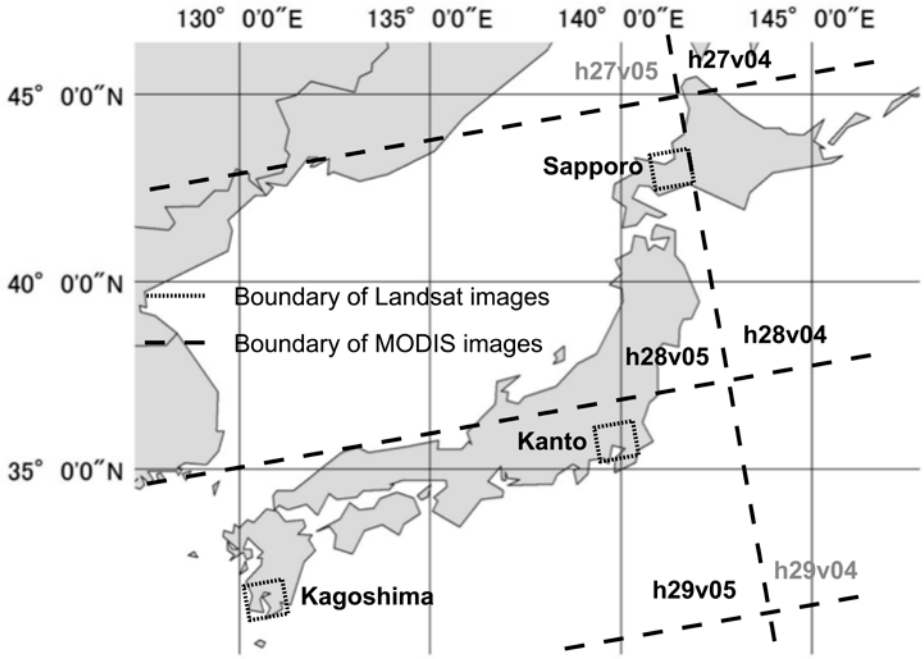

Figure 1: Location of the study area. Four MODIS tiles (h27v04, h28v04, h28v05 and h29v05) cover four main islands of Japan. Sapporo City, the Kanto Plain and central Kagoshima Prefecture were chosen for accuracy assessment.

(a)

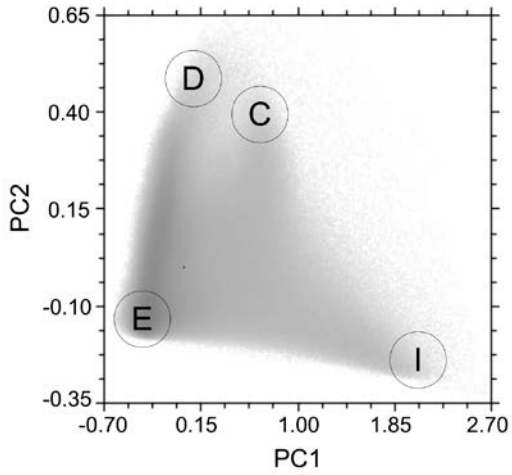

(b)

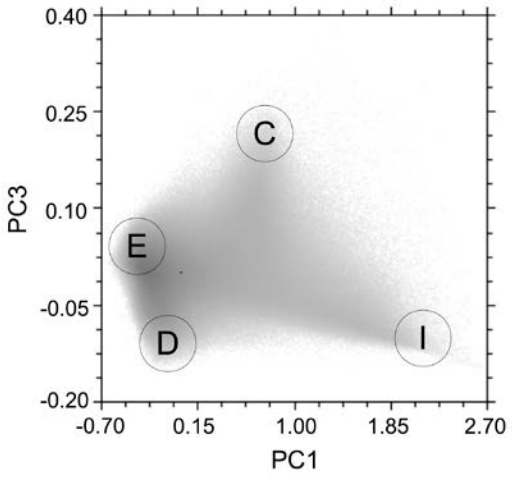

Figure 2: Feature space representations of the first three principal components. Four endmembers are found: E- evergreen forest, D- deciduous forest, C- cropland, I- impervious surface.

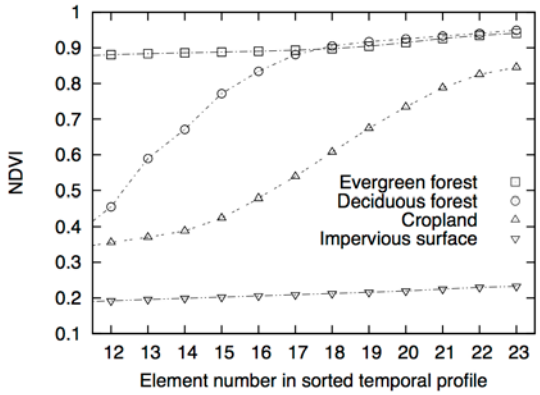

Figure 3: Temporal profiles of endmembers for sorted temporal mixture analysis

(a)

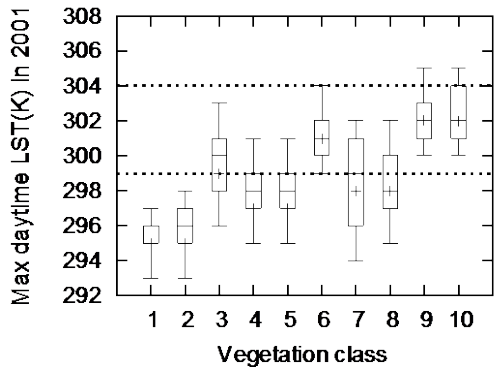

(b)

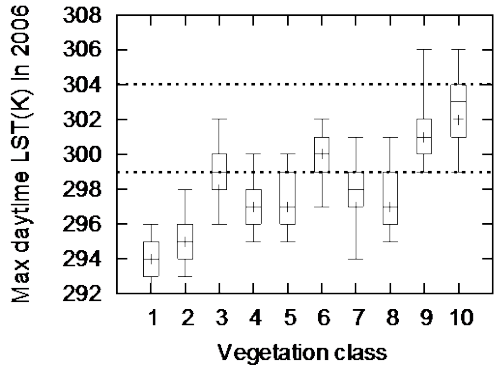

(c)

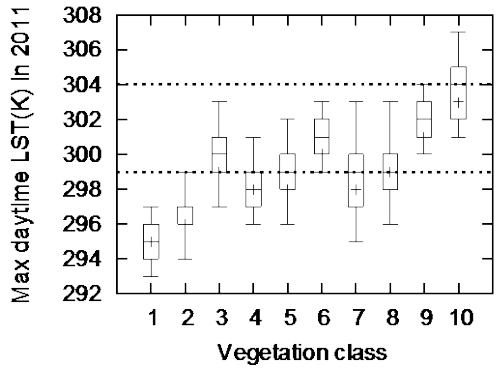

Figure 4: Summary statistics of yearly maximum land surface temperature for 10 main vegetation types in Japan. 1- alpine scrub & snow patch community; 2- subalpine needleleaf forest; 3- evergreen needleleaf forest; 4- deciduous needleleaf forest; 5- evergreen broadleaf forest; 6- deciduous broadleaf forest; 7- wetland; 8- grassland; 9- bamboo; 10- crop. For each type, the 5%, 25%, 50% (median), 75%. 95% percentiles and mean value (marked as plus) are shown.

(a)

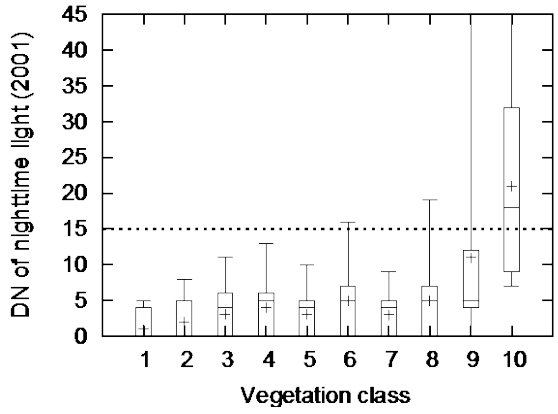

(b)

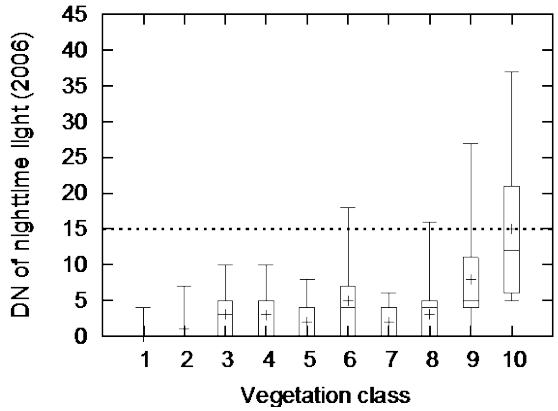

(c)

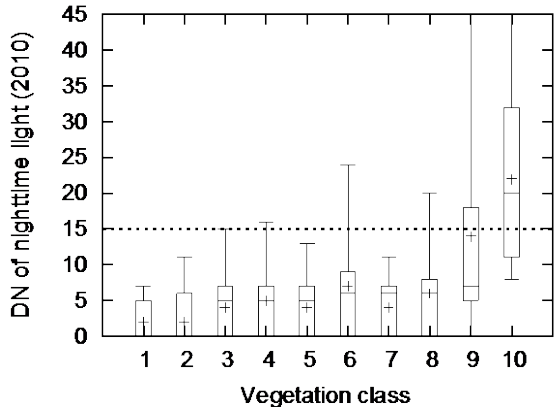

Figure 5: Summary statistics of averaged stable nighttime light for 10 main vegetation types in Japan, which are the same as those in Fig. 4. For each type, the 5%, 25%, 50% (median), 75%. 95% percentiles and mean value (marked as plus) are shown.

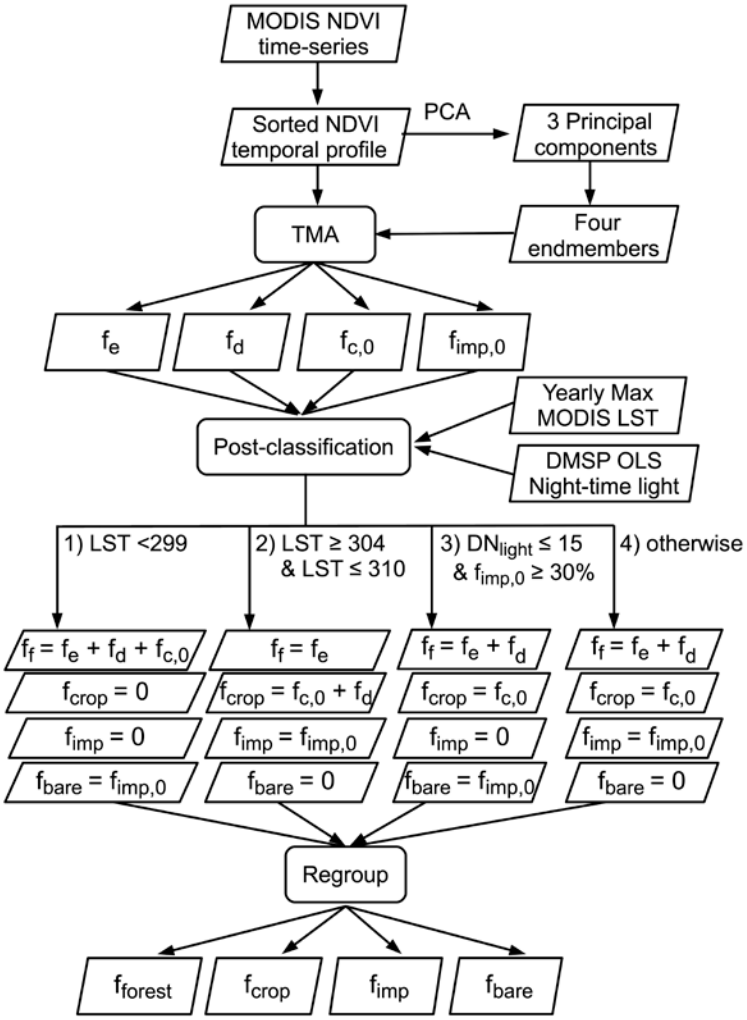

Figure 6: Flowchart of STMAP. f_e, f_d, $f_{c,0}$ and $f_{imp,0}$ represent the initial fractions of four endmembers (i.e., evergreen forest, deciduous forest, cropland and impervious surface) obtained from the sorted temporal mixture analysis, respectively. f_f, f_{crop}, f_{imp} and f_{bare} represent the four final results (i.e., fractions of forest, cropland, impervious surface and bare land) of STMAP. LST is the yearly maximum land surface temperature and DN_{light} represents the digital number of averaged stable nightlight light.

(a)

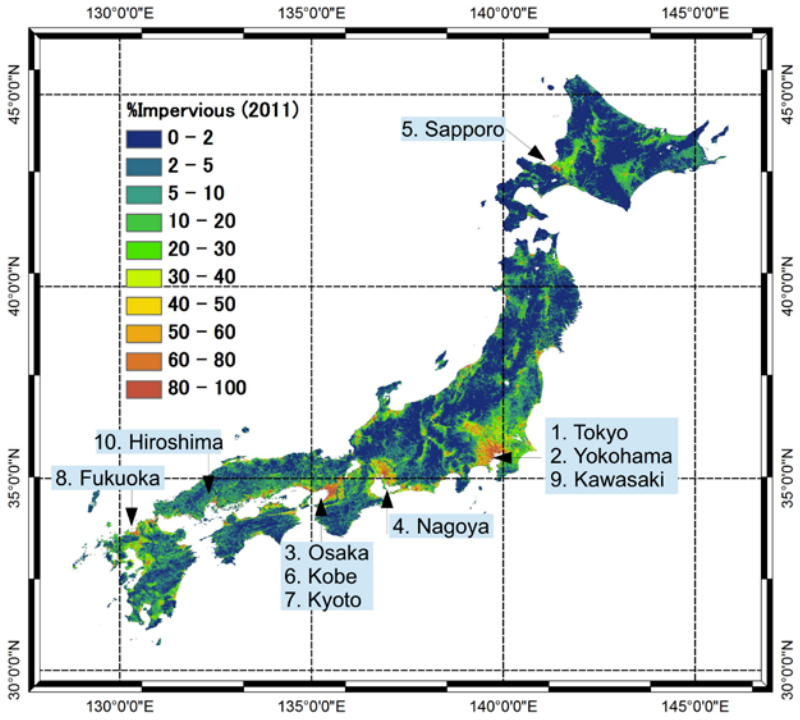

(b)

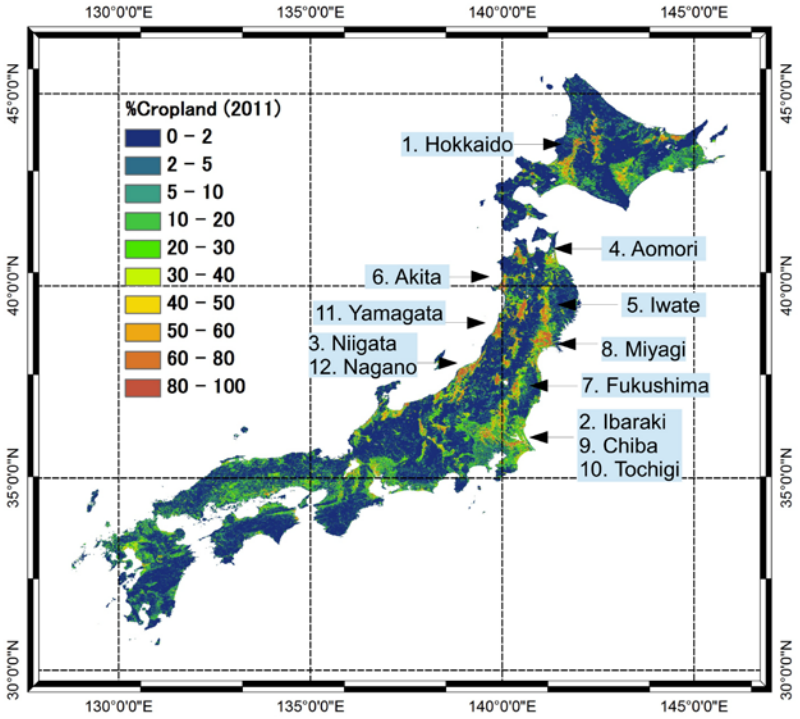

Figure 7: Distribution maps of impervious surface and cropland. (a) Estimated impervious surface. Top 10 cities (number is the rank) having the largest population are marked; (b) estimated cropland. Top 12 prefectures having the largest cropland are marked.

(a)

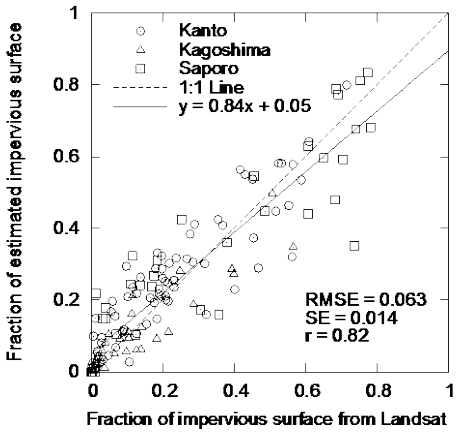

(b)

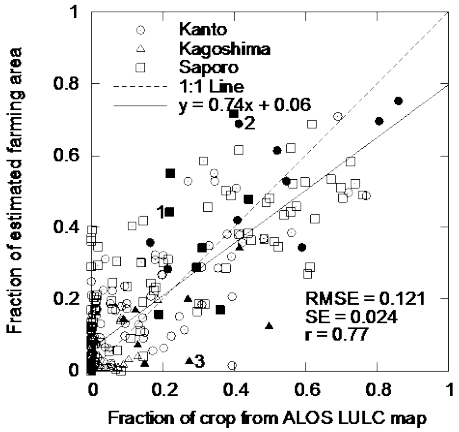

Figure 8: Accuracy assessment. (a) Accuracy assessment of impervious surface by comparing to the referenced maps made from Landsat images; (b) accuracy assessment of cropland by comparing to the ALOS LULC map. The points with number are chosen for visual comparison in Fig.9, and the filled points are randomly chosen for photo interpretation further in Fig.10.

(a) Window example 1 (b) Window example 2 (c) Window example 3

(d) %Impervious = 21.3% (e) %Impervious = 23.4% (f) %Impervious = 11.2%

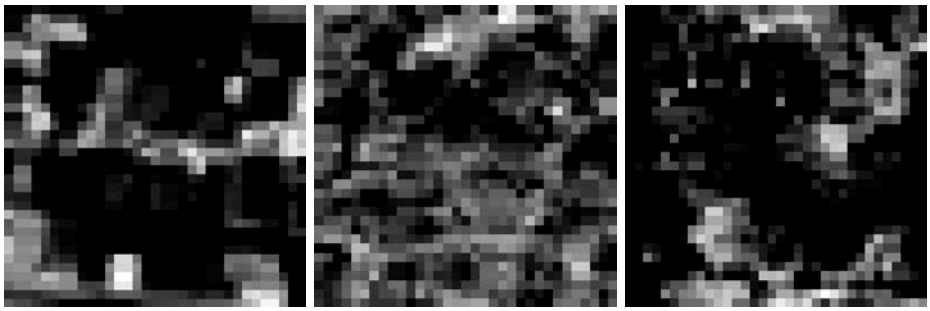

(g) %U = 0.0%, %C = 21.9% (h) %U = 18.8%, %C = 41.3% (i) %U = 0.0%, %C = 27.5%

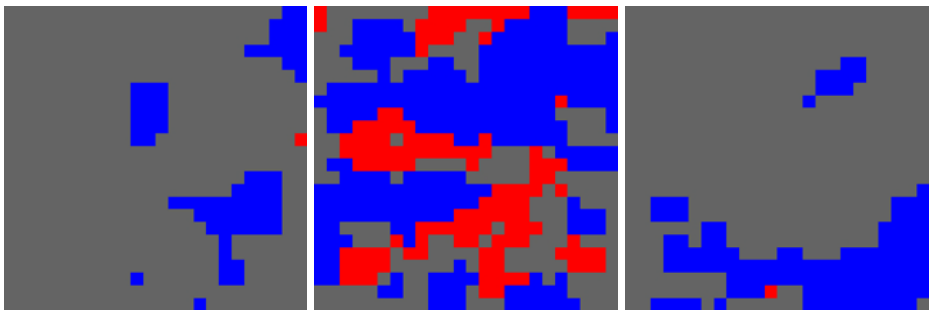

Figure 9: Three examples for visual comparison. a, b, c are the aerial photos for three assessment windows around 2011 in Google Earth, respectively; d, e, f are the reference maps of impervious surface generated from Landsat images for each window. g, h, i are from ALOS LULC map: the pixels classified as crop are in blue and urban in red for each window.

(a)

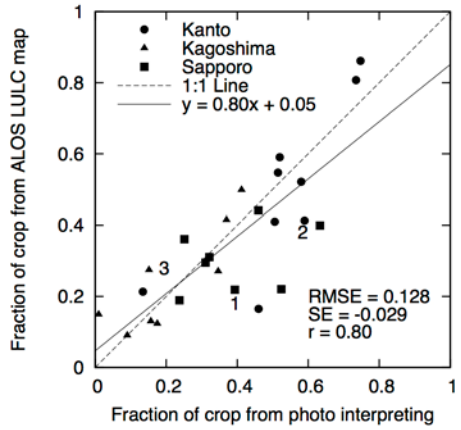

(b)

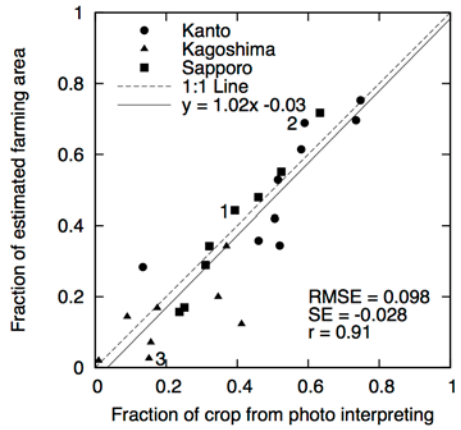

Figure 10: Accuracy assessment for 25 assessment windows. (a) Twenty-five sampled cropland windows referenced from ALOS LULC map are assessed by photo interpretation; (b) Twenty-five sampled cropland windows estimated by STMAP are assessed by photo interpretation. Points with number of 1, 2 and 3 are the results of window example 1, 2 and 3 shown in Fig. 8 and Fig.9, respectively.